# Quantification characterization of micropores in G20Mn5N cast steel at two different stages



IOP Conf. Series: Materials Science and Engineering **592** (2019) 012085 doi:10.1088/1757-899X/592/1/012085

# Quantification characterization of micropores in G20Mn5N cast steel at two different stages

**Huadong Yan[1], Hui Jin[1]***

[1]Jiangsu Key Laboratory of Engineering Mechanics, Department of Civil Engineering, Southeast University, Nanjing 211189, China

jin hui@seu.edu.cn

**Abstract**. Cast steel is an important metal material that is widely used in civil engineering structures due to its high strength and good ductility. However, a variety of casting defects such as micropores are usually present in the as-cast components. Casting defects are the main factors leading to the degradation of mechanical properties. In this paper, X-ray tomography is used to quantify the quantity, size distribution of micropores in G20Mn5N cast steel. In the nine notched samples, the quantity of pores increases from 2726 in the undeformed stage to 6440 in the fractured stage. Compared with the undeformed stage, the total volume and the average volume of the micropores in the fractured stage are also increased. Furthermore, the distribution of equivalent pore diameter of the two stages is studied, which is consistent with the three-parameter lognormal distribution.

## 1. Introduction

Steel castings are structural components made from cast steels, which are widely used in civil engineering structures, especially as connection joints of the large-span steel structures. Compared with regular welded joints, cast steel joints have a streamlined shape for minimum stress concentrations, and have a good degree of design freedom. However, due to the effects of alloying elements, casting temperature, spheroidizing graphite and post heat treatments, cast steel almost always contains some microscopic casting defects, such as pores, hot cracks, oxide skins, and flux inclusions[1,2]. One of the typical casting defects is micropores, which lead to microstructural discontinuities and adversely influence the structural durability[3,4]. Although casting defects have these adverse effects on the mechanical properties of the steel castings, these defects cannot be completely avoided.

Traditional nondestructive evaluation methods such as ultrasonic testing can be applied to find macro casting defects in steel castings. However, the resolution of these methods is insufficient to determine the sizes and locations of micropores. The mechanical properties of materials are intrinsically determined by the chemical composition and microstructural features. Therefore, designers employ excessively high safety factors to eliminate the influence of micropores which resulting in components that are heavier than necessary[5]. It is important to study the properties of micropores clearly and profoundly[6]. With the developments of X-ray sources, optical devices and image analysis technology, X-ray tomography appears to be an effective tool that enables three-dimensional and nondestructive investigations of the microstructures of building materials[7,8] In this paper, X-ray tomography is used to investigate the quantity, size distribution of micropores in G20Mn5N cast steel. These analytical results have positive implications for the in-depth study of cast steel.

## 2. Samples and experimental procedure

### *2.1. Samples*

The material used in this paper is G20Mn5N cast steel, which has a combination of high strength and good ductility. The chemical composition (wt%) of G20Mn5N cast steel is C 0.17-0.23; Mn 1.00-1.60; Si ≤0.6; Ni ≤0.80; P ≤0.020 and S ≤0.020. The smooth samples and notched samples used in this paper are extracted from a casting ingot with dimensions of 250 mm×180 mm×60 mm. The smooth samples are used for macroscopic mechanical properties tests, and the notched samples are used for X-ray tomography. The shape and size of the smooth and notched samples are shown in Fig. 1. The thickness of these samples are 2 mm.

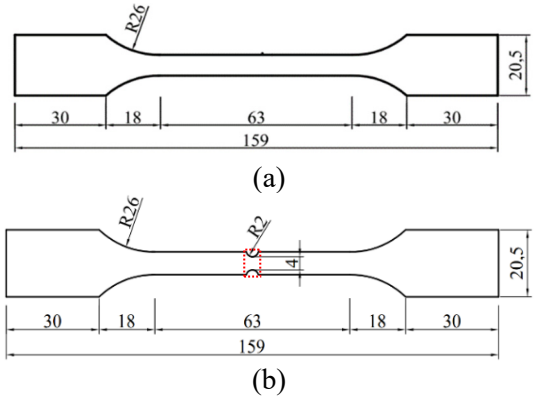


Figure 1. Tensile samples (units: mm): (a) Smooth sample, (b) Notched sample.

### *2.2. Tensile test procedures*

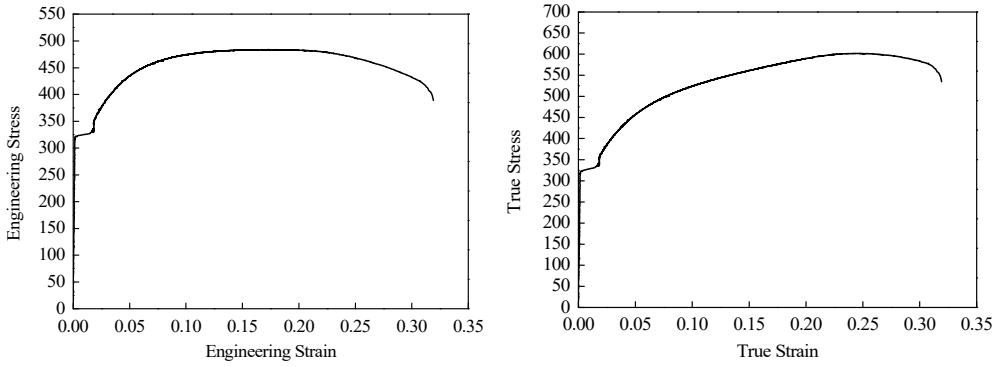


Figure 2. Stress-strain curves of G20Mn5N cast steel: (a) Engineering strain-Engineering stress curve, (b) True strain-True stress curve.

In order to investigate the macroscopic mechanical properties of G20Mn5N cast steel, uniaxial tensile tests of smooth samples are conducted using an INSTRON 3367 universal testing machine. The whole-field strain during the tensile test of smooth samples is measured by the 3D digital image correlation (DIC) technology. Performing the DIC analysis, the samples are painted in white colour and sprinkled with block dots to generate the random pattern. The samples are illuminated using halogen lamps to record high contrast images. The engineering and true stress-strain curves of this studied cast steel have shown in Fig. 2. The elastic modulus of G20Mn5N cast steel is 230 GPa, and the yield stress is 320 MPa.

### *2.3. X-ray Tomography observations*

Table 1. Parameters used in X-ray tomography.

| Sample | Pixel [mm] | Voltage [kV] | Current [mA] | Prefiltration Al [mm] | Exposure time [ms] | Number of projections |
|---|---|---|---|---|---|---|
| 1-9 | 0.016 | 195 | 0.29 | 1 | 2000 | 1350 |

Tensile tests coupled with X-ray tomography are used to detect the micropores in the undeformed stage and the fractured stage of the notched samples. The uniaxial tensile tests are conducted by use of an INSTRON 3367 universal testing machine. The scanned setup is a Y.CT Precision System, which is equipped with a 225-kV X-ray source and a Perkin Elmer XRD 0820 16-bit amorphous silicon sensor with a flat-panel detector that produced images of 1024×1024 pixels. When the notched sample is scanned, the tensile test will be interrupted.

All the notched samples are scanned under the same measurement conditions. To obtain the maximum measurement resolution, only the centre of each notched samples is reconstructed (dashed line in Fig. 1(b)). During scanning, the X-ray beam is filtered using a 1-mm Al filter to reduce beam-hardening effects. The parameters are set based on the density and size of the tested samples. The scanning parameters are shown in Table 1. Using software package VG-Studio Max 3.0 to process experimental data.

## 3. Analyses of tomography results

In this study, the quantity and size distribution of micropores in the undeformed state and in the fractured stage are compared. The 3D shapes of pores can be characterized by the ratio of the surface area of the equivalent volume to the actual surface area of the pores[9]. This value is defined as sphericity $C$, which is expressed as follows:

$$C = \sqrt[3]{\frac{36\pi V^2}{s^3}} \tag{1}$$

where, $V$ is the actual volume of the pore and $s$ is the actual surface area of the pore. For the ideal sphere, $C$ is equal to 1.

### *3.1. Quantity Comparison of micropores*

A statistical information of the micropores in the notched samples 1-9 is given in Table 2, and the 3D reconstruction results of the X-ray tomography of Sample 1 and Sample 8 at two different stages are shown in Fig. 3. To reduce the influences of measurement noise and artifacts, micropores less than 20 voxels in volume are neglected in the analysis. The volume of the smallest pores detected in each notched samples is $7\times10^{-5}$ mm$^3$.

In the undeformed stage, a total of 2726 pores are detected. The average volume of these pore is 0.00037 mm3, the average surface area is 0.04498 mm$^2$, and the average sphericity is 0.49897. A total of 6440 pores are detected in the fractured stage of the 9 notched samples, and the total number of pores increased by 136.24% compared with the undeformed stage. The growth rate of the quantity of pores in the 9 notched samples is from 16.26% to 597.35%. The quantity of pores in Sample 7 increases the most, while the quantity of pores in Sample 3 increases the least. The average volume of all pores increases from 0.00037mm$^3$ in the undeformed stage to 0.00049 mm$^3$ in the fractured stage, and the sphericity increases from 0.49897 to 0.51491. It is noted that the average volume growth rate of the pores (32.43%) is much lower than the growth rate of the total volume of the pores (198.29%), which is due to the interaction between pores nucleation and pores growth. The nucleated new pores are very small, which will reduce the average volume of all pores, whereas pores growth increase the volume of pores. The growth rate of the pores volume fraction is 148.32%, which is approximately the same as the total volume growth rate of the pores.

Table 2. Characterization information for micropores in the 9 notched samples.

| Sample | Stage | Quantity | Fraction (%) | Volume ($mm^3$) | | Surface area ($mm^2$) | | Sphericity | |
|---|---|---|---|---|---|---|---|---|---|
| | | | | Max | Mean | Max | Mean | Max | Mean |
| 1 | Undeformed | 184 | 0.176 | 0.0036 | 0.0003 | 0.3191 | 0.0347 | 0.65 | 0.47 |
| | Fractured | 713 | 0.615 | 0.0070 | 0.0004 | 0.4442 | 0.0449 | 0.71 | 0.55 |
| 2 | Undeformed | 192 | 0.156 | 0.0034 | 0.0004 | 0.3889 | 0.0478 | 0.66 | 0.51 |
| | Fractured | 618 | 0.672 | 0.0310 | 0.0005 | 1.6626 | 0.0536 | 0.71 | 0.53 |
| 3 | Undeformed | 492 | 0.327 | 0.0047 | 0.0003 | 0.4643 | 0.0380 | 0.71 | 0.47 |
| | Fractured | 572 | 0.713 | 0.0196 | 0.0006 | 1.1482 | 0.0622 | 0.68 | 0.52 |
| 4 | Undeformed | 398 | 0.484 | 0.0465 | 0.0005 | 2.7835 | 0.0570 | 0.68 | 0.49 |
| | Fractured | 704 | 0.589 | 0.0567 | 0.0004 | 3.3180 | 0.0465 | 0.68 | 0.49 |
| 5 | Undeformed | 420 | 0.373 | 0.0106 | 0.0003 | 0.8136 | 0.0349 | 0.72 | 0.50 |
| | Fractured | 743 | 0.773 | 0.0856 | 0.0006 | 3.2916 | 0.0518 | 0.69 | 0.51 |
| 6 | Undeformed | 331 | 0.276 | 0.0044 | 0.0004 | 0.4240 | 0.0437 | 0.67 | 0.52 |
| | Fractured | 828 | 0.590 | 0.0340 | 0.0003 | 1.7753 | 0.0409 | 0.71 | 0.50 |
| 7 | Undeformed | 151 | 0.184 | 0.0037 | 0.0004 | 0.2957 | 0.0517 | 0.69 | 0.52 |
| | Fractured | 1053 | 0.748 | 0.0105 | 0.0003 | 0.5891 | 0.0406 | 0.71 | 0.51 |
| 8 | Undeformed | 368 | 0.307 | 0.0049 | 0.0004 | 0.4943 | 0.0458 | 0.71 | 0.53 |
| | Fractured | 822 | 0.674 | 0.0075 | 0.0004 | 0.5712 | 0.0437 | 0.71 | 0.52 |
| 9 | Undeformed | 190 | 0.300 | 0.0333 | 0.0006 | 2.1244 | 0.0626 | 0.70 | 0.51 |
| | Fractured | 387 | 1.040 | 0.1667 | 0.0012 | 7.4816 | 0.0898 | 0.68 | 0.52 |

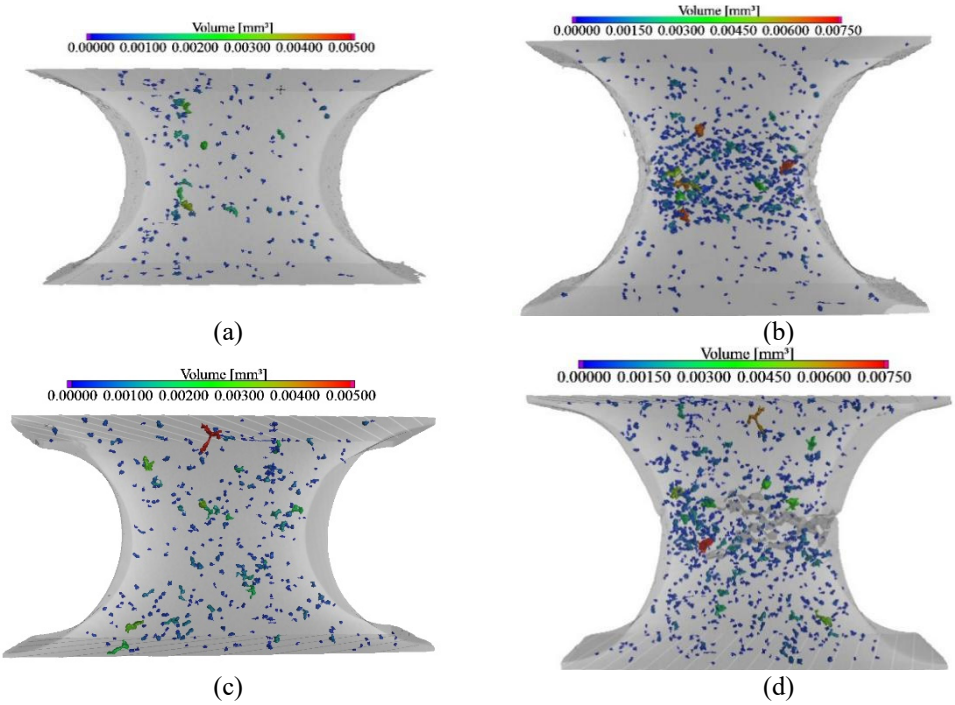


Figure 3. Micropores inspected with 3D X-ray tomography technology in the sample gauge section: (a) the undeformed stage of Sample 1, (b) the fractured stage of Sample 1, (c) the undeformed stage of Sample 8, (d) the fractured stage of Sample 8.

### *3.2. Distribution statistics of micropores*

It is important to statistically analyze the distribution of the equivalent diameter of casting micropores because this information is a basis for understanding of the influence of the pores on the mechanical properties of the material[10]. Dvorak H R[11] stated that, theoretically, the size of casting defects should follow a lognormal distribution. However, the research of Tiryakioğlu M[10] showed that the pore size

is better fitted by a three-parameter lognormal distribution than by a two-parameter lognormal distribution. The three-parameter lognormal statistics function can be written as follows:

$$g(x)=\frac{1}{(x-\tau)\sigma\sqrt{2\pi}}\exp\left[\frac{-\left(\ln(x-\tau)-\mu\right)^2}{2\sigma^2}\right] \tag{2}$$

where, $\mu$ and $\sigma$ are the logarithmic mean value and standard deviation of the pore size, respectively, $\tau$ is the threshold. The values of $\mu$ and $\sigma$ in Eq. (2) are estimated using the measured pore size data.

The Anderson-Darling statistic can be used to check the goodness of fit. The smaller the Anderson-Darling statistic is, the better the fit[12]. The Anderson-Darling statistic can be expressed as follows:

$$A^2=-n-\frac{1}{n}\sum_{i=1}^{n}(2i-1)\left[\log(P(x_i))+\log(1-P(x_{n-i+1}))\right] \tag{3}$$

where, $n$ is the number of pores to be fitted, $i$ is the order of the pores arranged by volume from small to large, and $P(x_i)$ is the cumulative probability.

The statistical distribution of the experimentally obtained equivalent pore diameters is studied using the cumulative distribution function corresponding to Eq. (2). The results are shown in Fig. 4. Table 3 gives the fitting parameter for the two different stages. $A^2$ for the three-parameter lognormal distribution in the undeformed stage is 35.15, which is significantly greater than 23.31 for the fractured stage. Therefore, the equivalent pore diameter of G20Mn5N cast steel in the fractured stage is more subject to the three-parameter lognormal distribution than that in the undeformed stage. The threshold pore diameter in the undeformed stage is 62.23 μm, and the value is 61.64 μm in the fractured stage. These two parameter values indicate that the minimum diameter of pores detected in the undeformed stage and the fractured stage of this studied cast steel is 62.23 and 61.64 μm respectively.

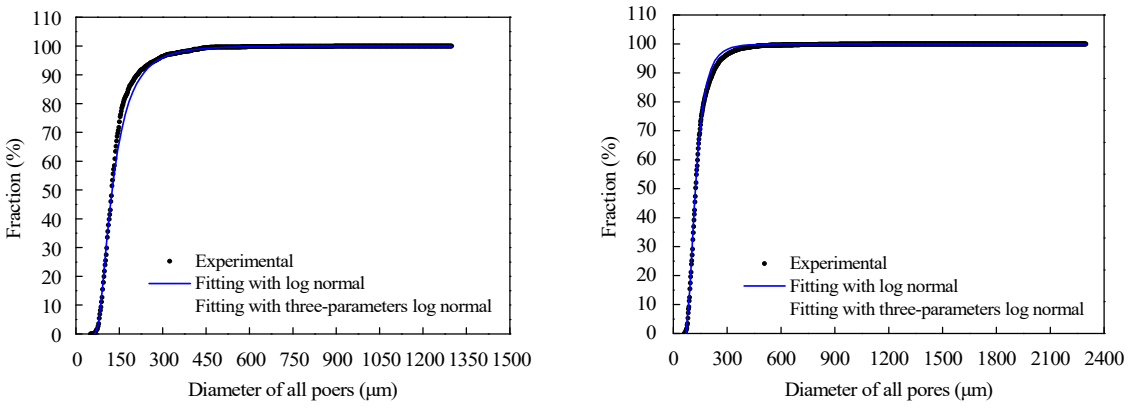


(a) (b)

Figure 4. Cumulative diameter based on three-parameter lognormal fitting: (a) in the undeformed stage, (b) in the fractured stage.

Table 3. Fitting parameter for the 3-parameter lognormal distributions.

| The undeformed stage | | | | The fractured stage | | | |
|---|---|---|---|---|---|---|---|
| $\mu$ | $\sigma$ | $\tau$ | $A^2$ | $\mu$ | $\sigma$ | $\tau$ | $A^2$ |
| 4.14478 | 0.75958 | 62.22781 | 35.15 | 4.10091 | 0.65843 | 61.64070 | 23.31 |

## 4. Conclusion

Micropores in G20Mn5N cast steel are detected based on X-ray tomography, and the obtained data is processed by software package VG-Studio Max 3.0. The quantity, size distribution of micropores in

the undeformed stage and in the fractured stage are compared. The following conclusions are drawn from this study.

A total of 2726 pores are detected in the undeformed stage of the 9 notched samples. With the accumulation of strain, the quantity of pores increases to 6440 in the fractured stage. The average growth rate of the pore quantity is 136.24%, and the pore quantity growth of each sample ranged from 16.26% to 597.35%. The average volume growth rate of the pores is 32.43%, while the growth rate of the total volume of the pores is 198.29%.

The equivalent diameter of casting pores in G20Mn5N cast steel at the fractured stage is more subject to the three-parameter lognormal distribution than that at the undeformed stage. The threshold of equivalent pore diameter in the undeformed stage is 62.23 μm, and the value is 61.64 in the fractured stage. These two parameter values indicate that the minimum equivalent diameter of pores detected in this studied cast steel is 62.23 and 61.64 μm respectively.

**Acknowledgements**
This work is supported by the National Natural Science Foundation of China (51578137), the National Key R & D Program of China (2017YFC0805100), the Open Research Fund Program of Jiangsu Key Laboratory of Engineering Mechanics, the Priority Academic Program Development of the Jiangsu Higher Education Institutions.

**References**

[1] Felberbaum M, Ventura T, Rappaz M and Dahle K 2011 *JOM* **63** 52
[2] Bacaicoa I, Wicke M, Luetje M, Zeismanna F, Brueckner-Foita A, Geisertb A and Fehlbierb M 2017 *Eng. Fract. Mech.* **183** 159
[3] Pysz S, Żuczek R, Piekło J and Maj M 2017 *Arch. Foundry Eng.* **17** 137
[4] Hardin R A and Beckermann C 2013 *Metall. Mater. Trans. A* **12** 5316
[5] Sigl K M, Hardin R A, Stephens R I and Beckermann C 2013 *Cast Met.* **17** 130
[6] Hardin R A and Beckermann C 2013 *Metall. Mater. Trans. A* **44** 5316
[7] Cao T S, Maire E, Verdu C, Bobadilla C, Lasne P, Montmitonnet P and Bouchard P O 2014 *Comput. Mater. Sci.* **84** 175
[8] Dong Y J, Su C, Qiao P Z and Sun L Z 2018 *Int. J. Damage Mech.* **27** 272
[9] Ziółkowski G, Chlebus E, Szymczyk P and Kurzac J 2014 *Arch. Civ. Mech. Eng.* **14** 608
[10] Tiryakioğlu M 2009 *Mater. Sci. Eng. A* **520** 114
[11] Dvorak H R and Schwegtier E C 1972 Int. J. Fract. Mech. **8** 110
[12] Tolikas K and Heravi S 2008 *Commun. Stat. Theory Methods* **37** 3135